



Article

Magnetic Properties of the Densely Packed Ultra-Long Ni Nanowires Encapsulated in Alumina Membrane

Daria Tishkevich ^{1,2,*} , Alla Vorobjova ³ , Dmitry Shimanovich ³, Egor Kaniukov ⁴, Artem Kozlovskiy ^{5,6} , Maxim Zdorovets ^{5,6,7} , Denis Vinnik ², Andrei Turutin ^{4,8} , Ilya Kubasov ⁴ , Alexander Kislyuk ⁴, Mengge Dong ⁹, M. I. Sayyed ^{10,11} , Tatiana Zubar ^{1,2} and Alex Trukhanov ^{1,2,*}

- ¹ Laboratory of Magnetic Films Physics, Scientific-Practical Materials Research Centre of National Academy of Sciences of Belarus, 220072 Minsk, Belarus; fix.tatyana@gmail.com
 - ² Laboratory of Single Crystal Growth, South Ural State University, 454080 Chelyabinsk, Russia; denisvinnik@gmail.com
 - ³ Department of Micro and Nanoelectronics, Belarusian State University of Informatics and Radioelectronics, 220013 Minsk, Belarus; vorobjova@bsuir.by (A.V.)
 - ⁴ Department of Technology of Electronic Materials, Department of Materials Science of Semiconductors and Dielectrics, National University of Science and Technology, «MISIS», 119049 Moscow, Russia; ka.egor@mail.ru (E.K.); aturutin92@gmail.com (A.T.); kubasov.ilya@gmail.com (I.K.); akislyuk94@gmail.com (A.K.)
 - ⁵ Engineering Profile Laboratory, L.N. Gumilyov Eurasian National University, Nur-Sultan 010000, Kazakhstan; artem88sddt@mail.ru (A.K.); mzdorovets@inp.kz (M.Z.)
 - ⁶ Laboratory of Solid State Physics, Institute of Nuclear Physics, Almaty 050032, Kazakhstan
 - ⁷ Department of Intelligent Information Technologies, Ural Federal University Named after the First President of Russia B.N. Yeltsin, 620075 Yekaterinburg, Russia
 - ⁸ Department of Physics and I3N, University of Aveiro, 3810-193 Aveiro, Portugal
 - ⁹ Department of Resource and Environment, Northeastern University, Shenyang 110819, China; mg_dong@163.com
 - ¹⁰ Department of Physics, Faculty of Science, Isra University, Amman 11622, Jordan; dr.mabualssayed@gmail.com
 - ¹¹ Department of Nuclear Medicine Research, Institute for Research and Medical Consultations (IRMC), Imam Abdulrahman bin Faisal University (IAU), Dammam 31441, Saudi Arabia
- * Correspondence: dashachushkova@gmail.com (D.T.); truhanov86@mail.ru (A.T.); Tel.: +375-29-562-8187 (D.T.); +375-29-518-6306 (A.T.)



Citation: Tishkevich, D.; Vorobjova, A.; Shimanovich, D.; Kaniukov, E.; Kozlovskiy, A.; Zdorovets, M.; Vinnik, D.; Turutin, A.; Kubasov, I.; Kislyuk, A.; et al. Magnetic Properties of the Densely Packed Ultra-Long Ni Nanowires Encapsulated in Alumina Membrane. *Nanomaterials* **2021**, *11*, 1775. <https://doi.org/10.3390/nano11071775>

Academic Editor: Filippo Giubileo

Received: 10 June 2021

Accepted: 6 July 2021

Published: 8 July 2021

Publisher's Note: MDPI stays neutral with regard to jurisdictional claims in published maps and institutional affiliations.



Copyright: © 2021 by the authors. Licensee MDPI, Basel, Switzerland. This article is an open access article distributed under the terms and conditions of the Creative Commons Attribution (CC BY) license (<https://creativecommons.org/licenses/by/4.0/>).

Abstract: High-quality and compact arrays of Ni nanowires with a high ratio (up to 700) were obtained by DC electrochemical deposition into porous anodic alumina membranes with a distance between pores equal to 105 nm. The nanowire arrays were examined using scanning electron microscopy, X-ray diffraction analysis and vibration magnetometry at 300 K and 4.2 K. Microscopic and X-ray diffraction results showed that Ni nanowires are homogeneous, with smooth walls and mostly single-crystalline materials with a 220-oriented growth direction. The magnetic properties of the samples (coercivity and squareness) depend more on the length of the nanowires and the packing factor (the volume fraction of the nanowires in the membrane). It is shown that the dipolar interaction changes the demagnetizing field during a reversal magnetization of the Ni nanowires, and the general effective field of magnetostatic uniaxial shape anisotropy. The effect of magnetostatic interaction between ultra-long nanowires (with an aspect ratio of >500) in samples with a packing factor of $\geq 37\%$ leads to a reversal magnetization state, in which a “curling”-type model of nanowire behavior is realized.

Keywords: porous anodic alumina; template synthesis; nickel; nanowire arrays; anodizing; electrodeposition; magnetic properties; magnetic anisotropy

1. Introduction

The development of the micro- and nanoscale systems, and the creation of the composite nanostructures, requires the study of the physicochemical properties of materials in nano-

volumes. Such material properties in an ultra-small volume (nanoscale clusters, nanowires, nanopillars, and other nanoelements and nanocomposites) differ significantly from the reference data for the bulk materials. In this regard, it is crucial to carry out experimental studies of the obtained nanostructures (nanocomposites) using known diagnostic methods. In addition, the accumulation of such knowledge will contribute to the intensive development of the experimental nanodiagnostic methods based on widely known developing, but still not exhausted, methods—atomic force microscopy, scanning electron microscopy (SEM), energy dispersive X-ray analysis, etc. The control of the structure and physical parameters of the obtained magnetic nanocomposites is also a very relevant problem.

Another major challenge today is the development of reliable methods for the fabrication of nanomaterials and nanostructures. The most promising methods are template synthesis and the self-organization principles since they are inexpensive and straightforward [1–4]. The primary attention of researchers is focused on the electrochemical synthesis of nanostructures and nanowires (NW) based on them using porous materials as a template. Porous materials (substrates) such as films of nanoporous anodic alumina [5–7], mica with etched nuclear tracks [8], polymer membranes [9,10], two-block copolymers [11], porous glasses with a nanochannel array of holes, and SiO₂ with nanocapillary pores [12–14] are used as porous templates. It is possible to form the arrays of parallel NWs using these porous materials as a template and multilayer NWs by changing the conditions of electrodeposition (voltage, current, electrolyte composition) [15,16]. The most popular porous nanomaterials applied as templates for obtaining NWs are track membranes, two-block copolymers with hexagonally ordered pores, and nanoporous alumina. All of them have a nanochannel structure with parallel to each other channels. However, among these materials, only nanostructured porous alumina is insoluble in organic solvents, resistant to high temperatures, and its geometric characteristics can be easily adjusted by the synthesis conditions changing [17]. However, only this template is considered as the most relevant for the structures based on NWs' integration into silicon technologies in a microelectronic production [15,18–23].

The deposition of ferromagnetic materials into the pores of the templates makes it possible to create macroscopically large areas of irregular and quasi-regular magnetic nanoscale elements: nanodots, nanopillars, nanowires [19–24]. In this case, the collective modes of the ferromagnetic quasiperiodic structure play an essential role in the mechanisms of an interaction of the magnetic field with the samples. Moreover, the nature of the exhibit of the magnetic effects is determined by both the dipole interaction between nanowires and the magnetic properties of individual nanoelements [25,26]. An experimental study of the effect of dipole interaction in the nanoparticles ensemble revealed many new phenomena that determine the collective behavior of the particles, which require further investigation [27,28]. In this regard, the precise control of their length and uniformity is essential for the practical application of NWs.

A number of studies have shown that obtaining the uniform length of NWs is influenced by such parameters of the electrodeposition process as membrane thickness, pore diameter, electrolyte composition, deposition duration, signal shape, etc. [29–32]. To achieve the full and uniform pore filling, three different methods are still being optimized: DC deposition, potentiostatic deposition [33], AC deposition [34], and pulsed electrodeposition [30,35]. A constant voltage supplies the DC deposition. It allows the deposition rate to be increased by controlling the overvoltage. The optimization of this process to increase the deposition rate will allow in the future the move to the industrial production of large and ordered arrays of high-quality nanostructures in a fast and uncomplicated manner.

Previous reports on electrodeposition optimizing of Fe [36], Cu [37], and Ni [38] in membranes based on porous anodic alumina (MPAA) to obtain defect-free NWs refer to a limited range of applied voltages (from ~− 0.7 to − 1.2 V vs. Ag/AgCl). In addition, many authors have studied the effect of stirring on Ni deposition in the MPAA [39], the waveform of the applied potential [40], the type of electrolyte, its concentration, temperature, and pH [41]. However, we found only one previous study about optimizing Ni

electrodeposition in the MPAA at long-term high negative overvoltages (lower than 2.0 V relative to Ag/AgCl) [30]. The main questions that arise at such potential, which, as a rule, corresponds to a higher current density, is at what voltage will the oversaturation of H₂ be achieved and how will it affect the formation of Ni NWs and the structural and magnetic properties of the deposits? Establishing such a limiting potential (or current density) would make it possible to fabricate arrays of long and uniform Ni NWs with a shorter duration of electrodeposition.

Additionally, it was shown in a number of works that the magnetic properties (coercivity and squareness) of the long NWs noticeably depend not only on the diameter, but also on the length of the NWs, as well as on the packing factor P of the volume fraction of the NWs in the MPAA [42–44].

In this regard, the development of the low-cost technological processes for the preparation of magnetic nanocomposites based on porous anodic aluminum oxide with magnetic filler in the form of long NWs is still actual. No less important is determining factors affecting the NWs' magnetic properties with different geometric parameters.

In our previous article [23], we presented the experimental results about the influence of the synthesis conditions on the magnetic behavior of the densely packed arrays of the Ni nanowires in the MPAA. The effect of the porous alumina membrane and the Ni NWs' synthesis conditions on the magnetic characteristics of Ni nanowire arrays has been studied. A previous paper describes the morphology, microstructure and magnetic properties of electrodeposited nanocrystalline Ni nanowires with a 6–12 μm length. Moreover, it was shown that with prolonged deposition under the simplified conditions, the formation of a NiO phase is possible, which leads to a degradation in the magnetic parameters of the NWs. Therefore, in the presented work, a new goal was set—a quick production of the ultra-long nanowires of high quality using conventional equipment.

In this regard, the purpose of this work is as follows: i. the development of a simple method, as close as possible to industrial production, for the manufacture of spatially ordered arrays of Ni NWs with different lengths using the MPAA as a template; ii. The determination of the optimal synthesis conditions for obtaining ultra-long Ni NWs with an aspect ratio of up to 700 using non-lithographic methods based on the self-organization principles; iii. The investigation of the influence of the geometric parameters of the MPAA and the NWs themselves on the magnetic properties of the Ni NW array in the MPAA.

2. Materials and Methods

The self-made membranes were used in this work. The MPAA were prepared using a specially designed A1 thick-layer anodizing unit. An aluminum foil (99.995%) of 100 μm thickness was used as raw material, from which substrates of 60 × 48 mm size were formed by mechanical cutting. The high-ordered MPAA with thicknesses of 55, 65, 75 μm were produced using two-step anodizing in a potentiostatic regime at the (40 ± 2) V voltage. An electrolyte of the following composition was used: 5% H₂C₂O₄ + 10 g/L MgSO₄ + 5 g/L C₆H₈O₇ + 5 g/L H₃BO₃ + 20 mL/L C₃H₈O. This electrolyte makes it possible to increase the anodizing rate of the MPAA obtaining and improve the membrane quality. The etching of the barrier layer was performed using two steps: i. etching in Ar plasma; ii. the barrier layer chemical etching and broadening of the MPAA pores in a 5% aqueous solution of H₃PO₄ at a temperature of (35 ± 2) °C for 20 min. An electron beam sputtering technique using the “Oratoriya” facility (01NE-7-004) (Kaliningrad machine-building factory, Kaliningrad, Russia) was used for the thin metal film (Ti) obtaining. The MPAA backside was coated with a chemically resistant varnish before the NWs electrodeposition. The process of a free MPAA manufacture is described in more detail in our previous works [45,46].

The galvanostatic electrodeposition mode at a direct current was used for the arrays of Ni NW preparation in MPAA. All experiments were carried out at a (28 ± 2 °C) temperature at a constant current density (1.0–4.0 mA/cm²) and a different electrodeposition duration in a two-electrode cell. An auxiliary electrode based on a graphite plate was used. The electrochemical parameters of the process were controlled using a P-5827M potentiostat

(Measuring Instruments Factory, Gomel, Belarus). The error in measuring a potential during electrodeposition was no more than 1 mV, and the current—30 nA. However, since a two-electrode cell and a constant current density mode were used, a conventional power supply can be employed. Such a mode and equipment correspond to the research goal—to develop and investigate a process as close as possible to industrial conditions. Guided by the experience of applied electrodeposition, we used an electrolyte for the thin Ni film deposition [47,48], in which nickel hexafluorosilicate instead of nickel sulfate was used (to accelerate the deposition process) with the following composition (in g/L): (140) $\text{H}_{12}\text{F}_6\text{NiO}_6\text{Si}$ + (30) $\text{NiCl}_2 \cdot 6\text{H}_2\text{O}$ + (25) H_3BO_3 + (60) Na_2SO_4 . An HI-83141 pH meter (HANNA instruments) (HANNA Instruments, Smithfield, USA) was used to determine and adjust the electrolyte pH value at a level of 5.2. The stirring of the electrolyte was carried out with a magnetic stirrer MS-H280-Pro (DLAB Scientific Co., Ltd., Beijing, China) at a speed of 350 rpm.

In addition, immediately before the Ni electrodeposition, the MPAA was preliminary treated in concentrated 60% HNO_3 for 2–3 min at room temperature, washed in running distilled water, and dried with an air flow. Then, the treatment using ion etching in Ar plasma was carried out at an Ar-ion energy of 3 keV for 30 min. Thus, the use of a new electrolyte and additional technological operations makes it possible to speed up the process of NW deposition.

The Ni mass was determined using a Sartorius CP225D microanalytical electronic balance (Sartorius Lab Instruments GmbH & Co. KG, Goettingen, Germany) with an accuracy of 0.01 mg. Samples were weighed before and after metal electrodeposition.

The Ni nanowires in MPAA morphology were studied using SEM (JEOL USA JSM-6400) (JEOL USA, Inc., Peabody, MA, USA). X-ray diffraction (XRD) analysis of synthesized samples was performed on the DRON-3M diffractometer (Cu-K α) (NPO Burevestnik, St. Petersburg, Russia) at room temperature ($\lambda = 1.542 \text{ \AA}$).

The magnetic parameters were investigated at the temperature range of 4.2–300 K using the Liquid Helium Free High Field Measurement System (VSM) (Cryogenic Limited, London, UK) [49]. The applied magnetic field was $\pm 2 \text{ T}$, and the precision of the measurements for specific magnetization σ was $\pm 0.01 \text{ A} \cdot \text{m}^2 \cdot \text{kg}^{-1}$.

3. Results and Discussion

3.1. Morphology and Microstructure

Table 1 shows the topological parameters of the MPAA fabricated for the experiments. The sample type (and No.) was determined by the MPAA thickness and the pore diameter/distance between pores ratio (d_p/D_{int}). The filling factor of the MPAA pores or the porosity (P) depends on this ratio. The distance between the pores is equal to the cell diameter of the MPAA and depends only on the alumina-forming voltage. The oxide-forming voltage for all samples is the same and equal to $(40 \pm 2) \text{ V}$; therefore, the D_{int} for all samples is also the same and equal to $105 \pm 5 \text{ nm}$ [33,46]. The filling factor (or P) depends on the d_p of the alumina, which in turn depends on the etching mode of the barrier layer at the bottom of the MPAA pores.

The porosity P (or packing factor) of the initial MPAA was determined by the formula [33,48]:

$$P = \frac{\pi}{2} \frac{d_p^2}{D_{int}^2} \quad (1)$$

The technological parameters of the Ni NWs in MPAA preparation are presented in Table 2.

Figure 1 shows the SEM images of a cross-section of No. six experimental sample: Ni NWs with a length of $49.3 \text{ }\mu\text{m}$ in the MPAA with a thickness of $55 \text{ }\mu\text{m}$ and a pore diameter of $(70 \pm 5) \text{ nm}$ (inset in Figure 1B).

Table 1. The MPAA sample parameters prepared for investigations.

Sample Type	Sample No.	MPAA Thickness (H), μm	Pore Diameter (d_p), nm	d_p/D_{int} Relation	Porosity (P), %
I	1	65	60 ± 5	0.51–0.59	26–31
	2	55			
	3	65			
II	4	75	70 ± 5	0.59–0.65	36–42
	5	55			
	6	55			

* After etching of the barrier layer at the bottom of the MPAA pores.

Table 2. The main technological parameters of the preparation process of the Ni NWs in MPAA.

Sample Type	Sample No.	Ni NWs Length (L_{NW}), μm	Aspect Ratio (n)	Current Density (j), mA/cm^2	Deposition Duration (t), min	Ni Mass (M), mg/cm^2	Deposition Rate (V), $\mu\text{m}/\text{min}$
I	1	11.9 * 11 ± 0.5	170	1.0	120	2.37	0.099
	2	22.7 * 21.5 ± 0.9	320	1.5	60	1.94	0.189
	3	24.8 * 23 ± 1.0	350	2.0	120	4.39	0.191
II	4	31.7 * 30 ± 1.3	430	2.0	240	8.29	0.132
	5	41.8 * 40 ± 1.7	570	3.0	240	14.04	0.174
	6	49.3 * 48 ± 2.0	700	4.0	240	17.27	0.205

*—the values of the NWs length according to the SEM images data.

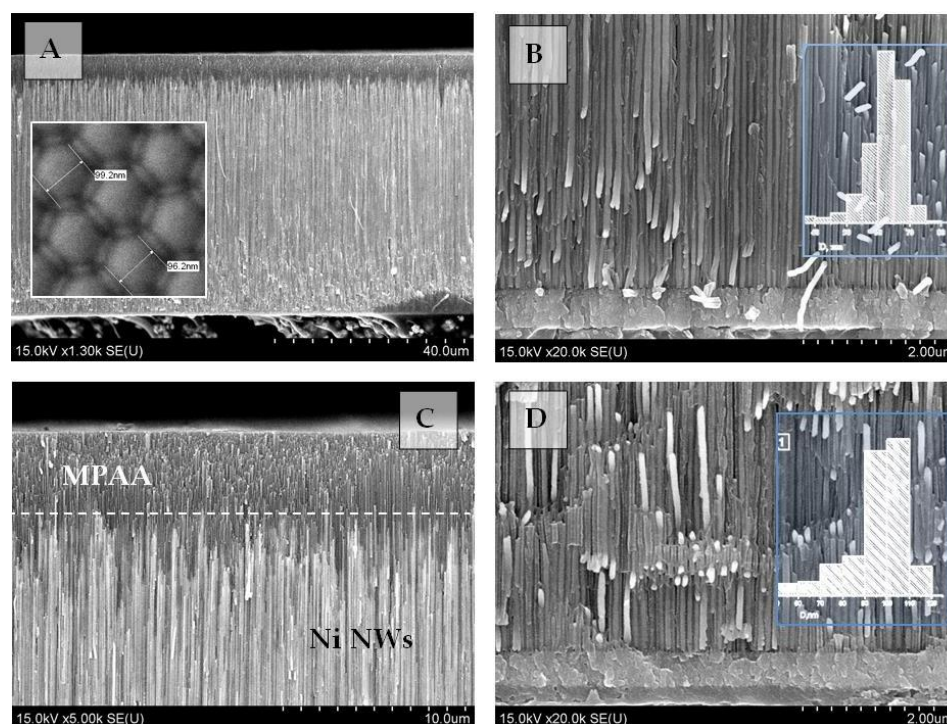


Figure 1. SEM images of the cross-section of the Ni NWs in MPAA (Sample No. 6): (A,C)—near the MPAA surface; (B,D)—near the bottom of the MPAA. The insets show the SEM images of the MPAA bottom (hexagonally packed oxide cells and their size) (A) and histograms of the diameter distribution (B) and the distance between NWs (D).

The hexagonally packed cylindrical nanowires (inset in Figure 1A) have a smooth wall surface and uniformly fill all the pores from the bottom of the MPAA to a certain height. The NWs are located only inside the MPAA pores and do not appear on the surface in all samples; that is, all magnetic and structural measurements refer exclusively to NWs in the MPAA. Figure 2 demonstrates the dependence of the Ni mass (m) on the current density for two values of the electrodeposition duration. As can be seen from Figure 2, the Ni m deposited in the pores of the MPAA more clearly depends on the current density value, and during the time it first increases, and then the process slows down.

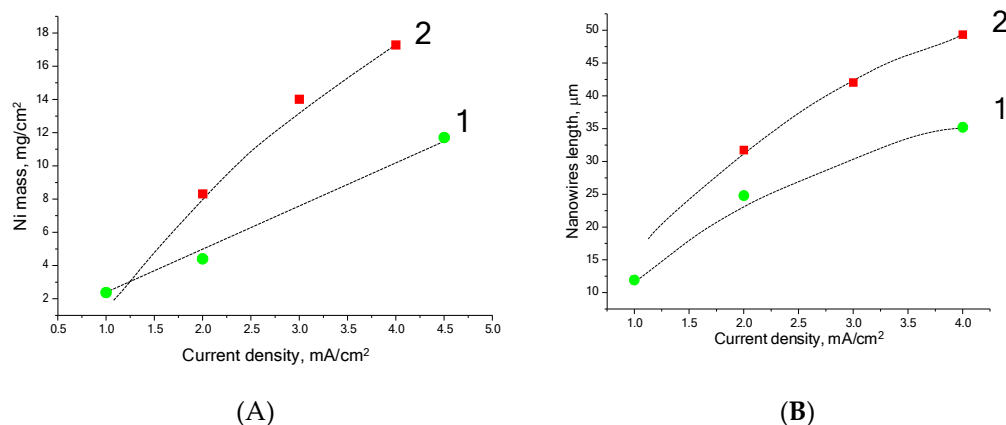


Figure 2. The dependences of the mass of the electrodeposited Ni (A) and the Ni NW length (B) on the current density at different deposition durations: 1—120 min; 2—240 min.

Arrays of the compact Ni NWs with different aspect ratios in the MPAA of 55–75 μm thicknesses at various current densities were obtained to refine and optimize the parameters of the electrodeposition process. Figure 3 presents the SEM images of the Ni NW experimental samples synthesized in the MPAA with 55, 65 and 75 μm thicknesses.

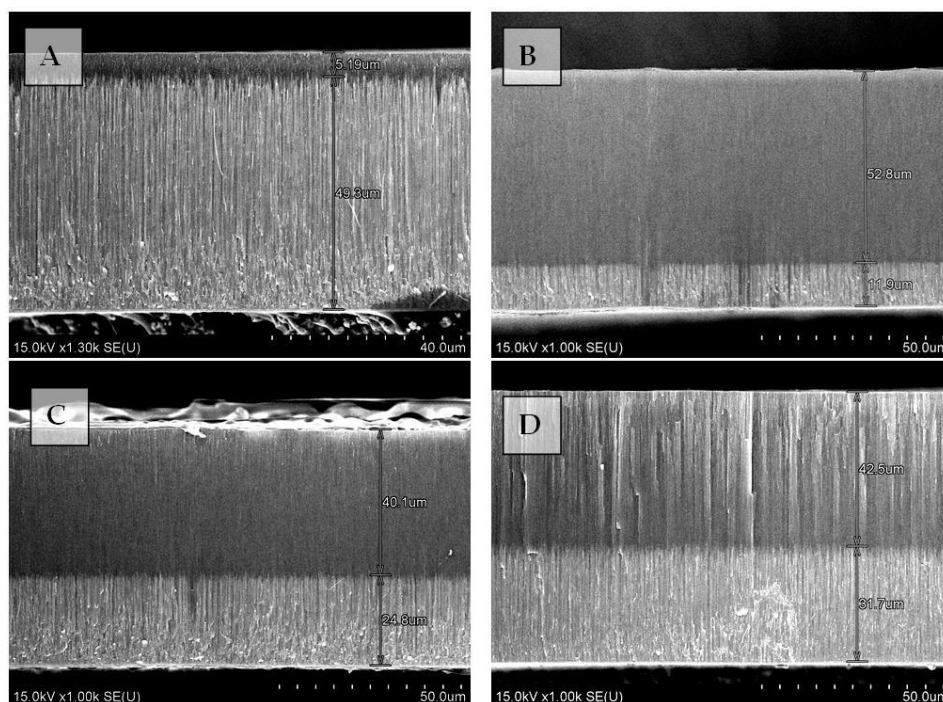


Figure 3. SEM images of the Ni NWs in MPAA pores of different thicknesses: (A)—55 μm, sample type II, No. 6; (B)—65 μm, sample type I, No. 1; (C)—65 μm, sample type I, No. 3; (D)—75 μm, sample type II, no. 4.

The dependence of the Ni NWs' aspect ratio ($n = L_{NW}/d_{NW}$) on the current density for various values of the MPAA thickness is shown in Figure 4.

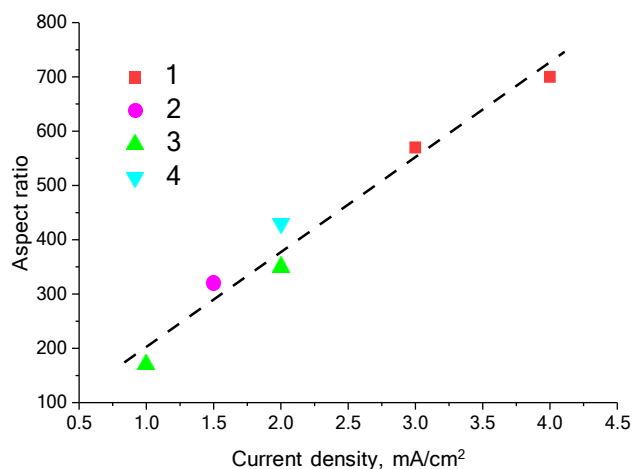


Figure 4. The dependence of the aspect ratio of the Ni NWs on the electrodeposition current density for different values of the MPAA thickness: 1—55 μm (Sample No. 5 and 6, type II); 2—65 μm (Sample No. 2, type I); 3—65 μm (Sample No. 1 and 3, type I); 4—75 μm (Sample No. 4, type II).

The dependence shown in Figure 4 presents that the aspect ratio of Ni NWs almost linearly depends on the current density and nearly does not depend on the MPAA thickness in the 55–75 μm range of thicknesses. Earlier obtained results [46] and new data of SEM images show that the quality of NWs (smoothness, uniformity in thickness, regularity) depends on the parameters of the electrodeposition process (j and t , that is, on the v), and on the quality of the MPAA. The uniformity of the electrodeposition process and the quality of the Ni NWs are the function of the MPAA quality and the rate of the pores filling with the metal.

3.2. Crystal Structure

The XRD spectra of the Ni NWs in the MPAA are shown in Figure 5. In Table 3, the parameters of the crystal structure of the Ni NWs are listed. The Ni crystallites average size calculation was carried out using the Debye–Scherrer equation.

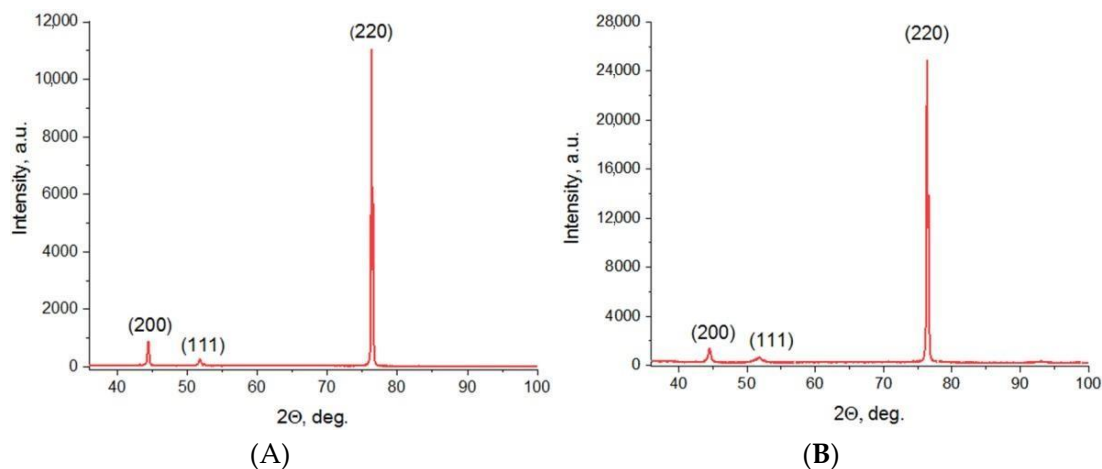


Figure 5. The XRD spectra for the Ni NWs in MPAA: (A)—I type (Sample 3); (B)—II type (Sample 4).

Table 3. The main parameters of the XRD spectra for the Ni NWs in MPAA for I and II sample types.

Sample Type	Sample No.	(HKL)	Intensity, %	2 θ , deg.	FWHM, deg.	Coherence Region
						Size (D), nm
I	3	220	100	76.33	0.36	16
		111	2.64	51.87	1.17	8
		200	5.46	44.50	0.53	28
		220	100	76.31	0.35	31
II	6	111	2.41	51.81	0.47	19
		200	7.98	44.44	0.28	29

The XRD spectra for the two types of samples are almost identical and differ only in the intensity of the signals, which are proportional to the length of the NWs. One main diffraction peak, which corresponds to the (220) cubic structure of Ni (Fm3m–PDF-2 card 270–989), is specific for all the investigated samples. However, there are also two weaker peaks corresponding to (111) and (200) Ni, which are specific for the Ni NWs in the MPAA.

The presence of the most intense peak with the (220) orientation indicates that Ni NWs have a high crystalline structure and crystallites mutually oriented along the main direction of growth. Therefore, the polycrystallinity of NWs was also observed since the existence of diffraction peaks with less intensity, which indicates a small amount of crystallites presence with other growth directions. Thus, it was concluded from the XRD data that NWs consist of the crystallites of Ni with a face-centered cubic structure. The main average size of crystallites was 21–29 nm, which is less in comparison with the Ni NWs' average diameter—(65–70) \pm 5 nm. It should be noted that the grain size of the NWs for samples of the I type (Sample No. 3) was approximately two times smaller than for the second type samples (Sample No. 6). This indicates the influence of the deposition conditions, particularly, the current density on the crystal structure of the deposit.

3.3. Magnetic Properties

The magnetic properties of the samples were measured with the magnetic field direction perpendicular and parallel to the sample surface. The perpendicular direction of the applied magnetic field to the MPAA surface corresponds to the direction parallel to the axis of the Ni NWs. The prepared samples were preliminarily weighed to determine the mass of the deposited Ni. The measurements and studies of the following magnetic properties of Ni NWs in the MPAA were carried out: remanent magnetization (M_r), saturation magnetization (M_s), coercivity (H_c), and the hysteresis loop squareness (M_r/M_s), depending on the magnitude and direction of the magnetic field and temperature. In this study, different lengths from 12 to 50 μm of Ni NWs were obtained. The experimental data for the four samples (they are named as one, three (I type), four, and six (II type), respectively) are presented in Figure 6.

It should be noted that for the correct calculations of the Ni NWs' magnetic characteristics we also measured an unfilled MPAA under the same measurement conditions. Then, the obtained magnetization data for a "clean" MPAA were subtracted from the data for samples with Ni NWs in the MPAA. It can be seen from Figure 6 that the squareness and broadening of the hysteresis loops were more when the applied magnetic field is parallel to the axis of the NWs. Then, the domains of Ni were located along the NWs' axis. This promoted the free reversal of domain magnetization vectors upon displacement of domain walls along to the magnetic field and induced the expansion and gain of the square shape of the hysteresis loops, especially for the samples of the I type. The obtained hysteresis loops showed that Ni NWs have a magnetization behavior characteristic of ferromagnets due to their axial shape anisotropy. The result of the axial anisotropy of the NWs shape was the existence of the two stable magnetic moment orientations, namely, in an antiparallel or parallel direction to the NWs' axis [50]. Thus, both types of samples are characterized by a predominant magnetic orientation along the axis of the NWs, i.e., axial anisotropy of the shape typical of ferromagnets such as Ni and Fe. The contours of the loops were more smoothed for the samples of the II type, which is usually explained by the enhancement

of the interaction between NWs. The information on the Ni NWs in the MPAA magnetic characteristics in comparison to both the polycrystalline bulk Ni and the results of other studies is listed in Table 4.

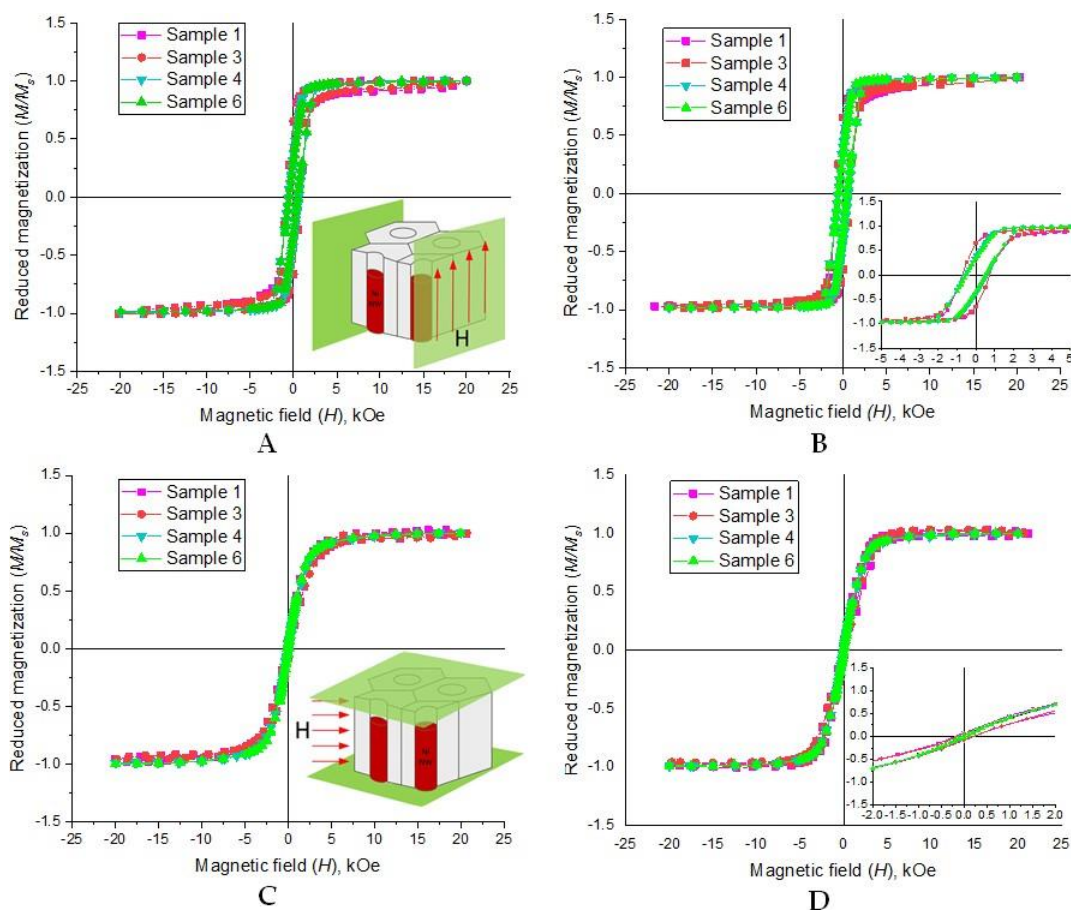


Figure 6. Normalized axial (A,B) and in-plane (C,D) hysteresis loops for Ni NWs at 4.2 K (A,C) and 300 K (B,D). The insets show increased magnetization fragments near zero H .

Table 4. A comparison of the coercivity and squareness of the hysteresis loops for Ni NWs in MPAA with different aspect ratios at 4.2 and 300 K temperatures.

Sample Type	Sample No.	Aspect Ratio	T, K	H_c, \parallel Oe	H_c, \perp Oe	$M_r/M_s, \parallel$	$M_r/M_s, \perp$
I	1	170	4.2	770	207	0.65	0.07
			300	723	182	0.66	0.08
	2	320	4.2	798	222	0.48	0.07
			300	756	208	0.51	0.07
	3	350	4.2	775	174	0.66	0.06
			300	727	138	0.65	0.06
II	4	430	4.2	603	94	0.41	0.04
			300	593	44	0.40	0.02
	5	570	4.2	574	73	0.42	0.03
			300	596	40	0.44	0.02
	6	700	4.2	515	95	0.35	0.05
			300	513	43	0.34	0.02
Ni NWs in Al_2O_3 template [51]			–	580	162	0.49	0.066
Ni NWs in Al_2O_3 template [52]			–	624	–	0.30	–
Bulk Ni [53]			–	100	–	0.49	–

The geometrical parameters of the Ni NWs from other references: [51]—NWs with a diameter of 70 nm in the alumina template with a thickness of 50 μm ; [52]—pore diameter of alumina $d_p = 50$ nm, the distance between pores $L = 100$ nm, diameter = 60 nm, length of NWs 12 μm ; [53]—bulk Ni with a 2–3 μm thickness.

Figure 7 shows the dependence of the H_c on the aspect ratio and temperature for two types of samples. It can be seen from the dependences that H_c for the samples of the II type (average filling factor is 39%) is less than for samples of the I type (average filling factor 28%), and at n greater than 500, it begins to decrease. This character of dependences may mean that the degree of the magnetostatic interaction between NWs rises with an increase in the NWs' length.

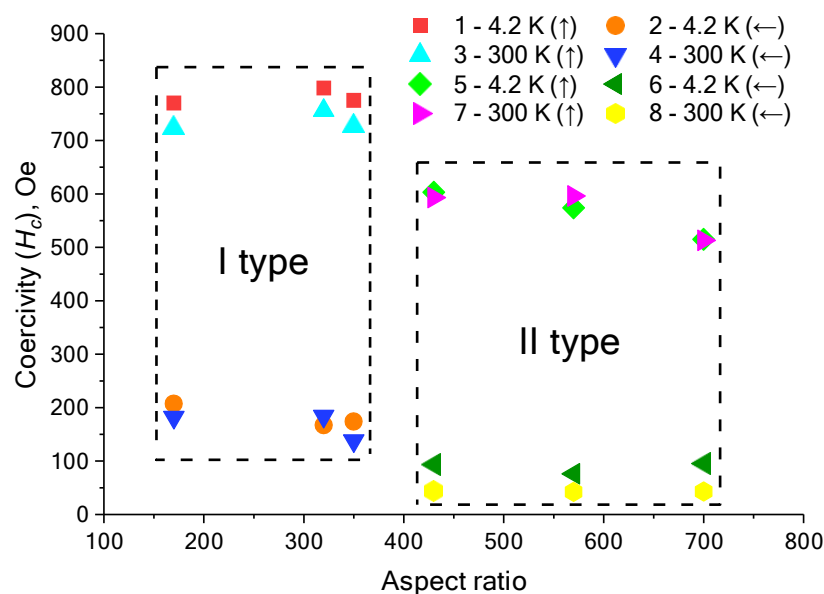


Figure 7. The dependence of the coercivity on the aspect ratio for two types of samples at 4.2 K and 300 K temperatures: 1, 2, 3, 4—the I type (Samples No. 1, 2, 3); 5, 6, 7, 8—the II type (Samples No. 4, 5, 6).

Figure 8 shows the dependence of the squareness ratio (M_r/M_s) on the aspect ratio and temperature for the samples of two types.

The character of the M_r/M_s dependence on the aspect ratio and temperature was approximately the same as for the H_c and shows the influence of both n and the filling factor P on the magnetic parameters. The coercivity reached up to 800 Oe at a parallel direction of the magnetic field, but at a perpendicular direction, the H_c was about 180 Oe for the samples of the I type. For the samples of the II type, these values were ~ 600 and ~ 40 Oe, respectively. The remanent magnetization and the squareness of the hysteresis loops also differ significantly. Typically, the interaction between NWs reduces the squareness ratio. Nevertheless, the given parameters are higher than those of bulk Ni [53] and are similar to the identical parameters for the Ni NWs in the Al_2O_3 template [51,52]. The values of the specific magnetization at 300 K were in the range of 42–46 emu/g which corresponds to the sizes of Ni nanocrystallites and the measurement conditions [54]. The specific magnetization for bulk Ni is 58.9 emu/g [55]. The magnetic moment of the Ni atom in NWs was determined from the obtained data, which is equal to (0.44–0.48) μ_B , while for the bulk Ni, it is equal to 0.62 μ_B [56]. The lower values of the specific magnetization and magnetic moment can be associated with both the magnetostatic interaction of NWs and with size effects, which, in turn, are determined by the size and shape of the NWs. As a rule, the M_s decreases if higher values of the external magnetic field are required for magnetization to saturation, which is typical of long NWs [57,58].

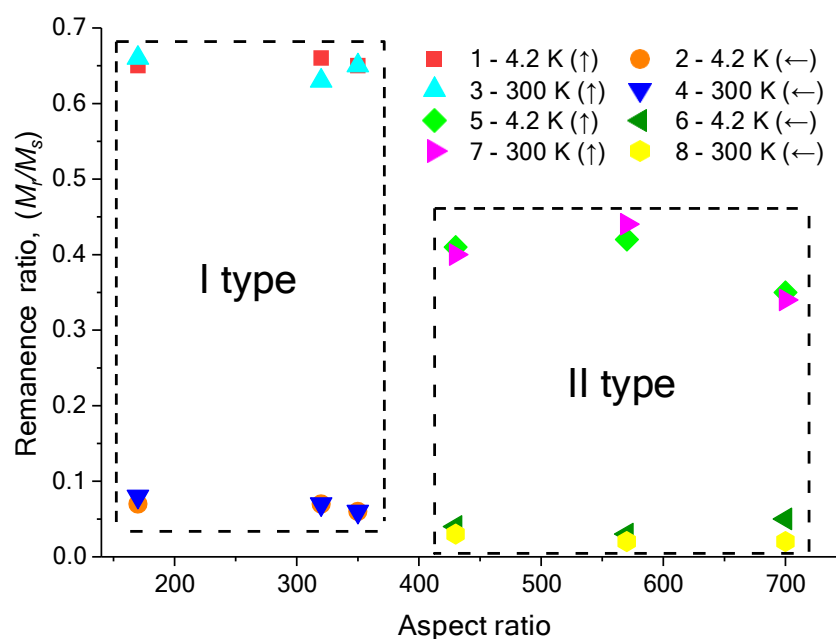


Figure 8. The squareness ratio M_r/M_s depending on the aspect ratio for two types of samples at 4.2 K and 300 K temperatures: 1, 2, 3, 4—the I type (Samples No. 1, 2, 3); 5, 6, 7, 8—the II type (Samples No. 4, 5, 6).

The saturation magnetization is a characteristic of the whole material (it depends on the atom's magnetic moment and their location in the NWs), while M_r , H_c , and the shape of the hysteresis loop are influenced by the NWs shape and size, taking into account the direction of the applied magnetic field [59].

Usually, an individual NW is considered as a single structural element, the influence on which of the other array elements is negligible since NWs interact with each other through weak dipole interactions [60]. This neglect of interaction is justified in the case when the density of the NWs in the array is low. In addition, the Ni NWs in the MPAA-based array are separated by thin walls of oxide cell. Therefore, the longer the length of the NWs and the thinner the walls of the MPAA (that is, the larger the pore diameter and, accordingly, the filling factor of the membrane), the stronger the effect of the interaction between the NWs. It can be seen from the data shown in Table 4 and Figures 7 and 8 that the magnetic properties of the experimental samples depend on the morphological parameters of the Ni NWs themselves and the MPAA. These parameters include: i. NWs' diameter (d_{NW}) and length (L_{NW}); ii. the d_p/D_{int} ratio, which determines the NWs' density (P_{NW}), porosity (P), and filling factor; iii. the ratio of a diameter to length of the NWs (d_{NWs}/L_{NWs}) (aspect ratio (n) or form factor). The density of the NWs, the number of NWs per unit volume of the MPAA, calculated according to the equation $P_{NWs} = \frac{2}{23D_{int}}$ [61] is approximately 10^{10} per cm^2 , and is uniquely related to the P , equal to 28% for samples of the I type and 39% for samples of the II type (Table 2). The degradation of the magnetic parameters of the II type samples indicates a change in the magnetic anisotropy due to the mutual magnetostatic interaction between NWs since this effect is proportional to the NWs' density [62].

A measure of the magnetic anisotropy is the energy of magnetization required to rotate the magnetization vector from a position parallel to the easy magnetization axis in the direction of the external field. The total anisotropy energy of the system consists of five components: the energy of crystal anisotropy (crystal lattice anisotropy), morphological anisotropy (anisotropy of the NWs geometric shape), mechanical stress anisotropy (magnetoelastic anisotropy), induced anisotropy (under the influence of the magnetic field), and exchange anisotropy. The magnetic properties of the NWs mainly depend on the magnetocrystalline anisotropy energy E_A and the demagnetizing field energy of the sample

E_D , which depends on its shape [59,60]. Magnetocrystalline anisotropy is a function only of the nature of the material and does not depend on the NWs' shape.

The magnetoelastic energy (and anisotropy) in nanostructures of the NWs' type turns out to be a too-small value. The energy of magnetocrystalline anisotropy makes a significant contribution in the case of single crystals or highly textured structures (for example, in Co NWs), but at the same time, it is much less than the contribution from the shape anisotropy. The energy of morphological anisotropy is of the greatest importance for the Ni NWs. An internal field H_{eff} (effective field of uniaxial anisotropy) during magnetization reversal of the NWs array actually turned out to be less than the external field H due to the demagnetizing field H_D and is equal to $H_{eff} = H - H_D$ [63]. The effective uniaxial anisotropy constant K_{eff} is given by:

$$K_{eff} = \pi M^2(1 - 3P) + K_u \quad (2)$$

The first term in this equation is due to the energy of the magnetostatic interaction of NWs (K_{eff} is due to the perpendicularly arrayed NWs' magnetostatic energy) [64]. The K_u constant considers some extra second-order uniaxial anisotropy with the symmetry axis along to the NWs' direction [65]. The packing coefficient P for a perfectly hexagonally ordered array of the NWs was determined with Equation (1). Actually, the effective uniaxial anisotropy, namely K_{eff} , should decrease linearly with P rising. This can lead to the axis of easy magnetization of the NWs to begin to rotate in the transverse direction.

Recently, the process of magnetization reversal of NWs has been considered within the framework of two models for single-domain nanoparticles: the coherent rotation model [60] and the "curling" model with the formation of a vortex magnetic field inside the NW (Figure 9) [66–68].

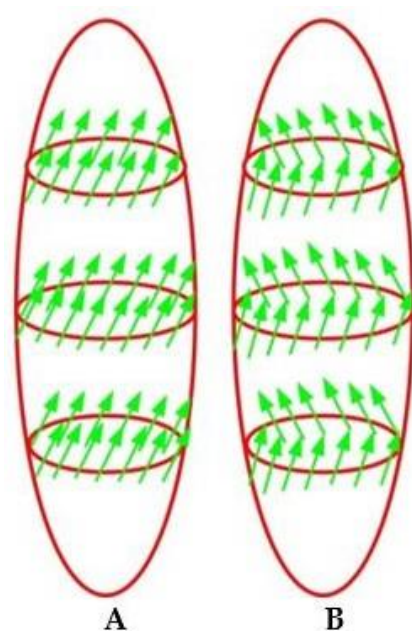


Figure 9. Models of the magnetization switching in a single-domain elongated spheroid: (A) coherent rotation of magnetic moments; (B) rotation of magnetic moments of the "curling" type [60,66].

Obviously, the method of the magnetization reversal depends on the size (diameter and length) and form factor (a.r.) of the magnetic NW. Theoretical and experimental studies have shown that for the Ni NWs, the significant magnetostatic interaction should be expected for the thick and closely spaced NWs. The conditions for the formation of such NWs can be realized, in particular, when using the MPAA as a template for the synthesis of the NWs array [69,70]. Thus, an analysis of the magnetostatic properties of the 2D NWs arrays and experimental results show that the dipole interaction in the NWs array depends

not only on the distance between them (determined by the MPAA), but also on the NWs' form factor [29,71–73].

Similar results were obtained in our study. The results obtained show that at $\approx 39\%$, the coercive field and squareness depended on the length of the NWs (or n) and on the NWs' diameter (or P) for the two types of samples. At $P \leq 28\%$, the coercive field and squareness were comparable with the same parameters for the NWs formed in the Al_2O_3 template in other works [74–76]. In addition, the weakening of the shape anisotropy of cylindrical NWs may be due to their imperfection (structural defects): the quality of the NW walls, polycrystallinity, the shape of the NWs' ends, and fluctuations in the diameter and distance between NWs [77]. It should be noted that this effect is not due to the properties of pure Ni, but is associated with the features of the electrodeposition process, for example, a high deposition rate for long NWs obtaining, or an uncontrolled rise in the electrolyte temperature, which leads to the formation of NWs with a rough wall surface [30].

Another reason is the experimental techniques used for the samples study—with or without the MPAA and/or with or without an aluminum substrate. In this case, with fluctuations in the external temperature, the weakening of the magnetic anisotropy and the change in the parameters of NWs with a rise in their length are associated with the appearance of magnetoelastic anisotropy, caused by the difference in thermoelastic characteristics of the Ni/MPAA composite material and the deterioration of the quality of the NWs with an increase in their length [78–81]. However, our NWs samples had smooth walls and a thin conducting Ti deposited on the backside of the MPAA. The aluminum substrate was etched away; therefore, the significant tensile stresses did not arise and magnetoelastic anisotropy did not appear. Thus, in our self-made samples, the NWs' length defined the degree of the magnetostatic interaction between them, which affected the coercivity and squareness of the densely packed Ni NWs arrays, the quality of which depends on the synthesis conditions of the MPAA and Ni NWs.

4. Conclusions

The densely packed arrays of the Ni nanowires with a high aspect ratio of up to 700 and pore diameters of $60_{\pm 5}$ nm (type I) and $70_{\pm 5}$ nm (type II) were fabricated using porous anodic alumina membranes via DC electrochemical deposition. A new electrolyte for the Ni electrodeposition and MPAA pretreatment were used, which significantly sped up the deposition process. It was shown that the aspect ratio of the Ni nanowires almost linearly depends on the current density and nearly does not depend on the MPAA thickness in the 55–75 μm range of thicknesses. The morphological studies presented the hexagonally packed cylindrical nanowires had a smooth wall surface and uniformly filled all the pores from the MPAA bottom to a certain height. The NWs were located only inside the MPAA pores and did not appear to the surface in all investigated samples; that is, all structural and magnetic measurements refer solely to NWs in the MPAA. Scanning electron microscopy and X-ray diffraction results showed that Ni nanowires are homogeneous and mostly a single-crystalline material with a 220-oriented growth direction. The main average size of crystallites was 21–29 nm. Therefore, under the presented deposition conditions, the NiO phase does not form in the NWs. The magnetic characteristics investigation showed the degradation of the magnetic parameters of the samples of the II type, which is associated with a change in the magnetic anisotropy due to the mutual magnetostatic interaction between NWs. The dipolar interaction between NWs in the array changed the demagnetizing field during a reversal magnetization of the Ni NWs, and the general effective field of magnetostatic uniaxial shape anisotropy. The effect of the magnetostatic interaction between ultra-long nanowires (with an aspect ratio of > 500) in samples with a packing factor of $\approx 37\%$ can lead to a reversal magnetization state, in which a “curling” model of the NWs' behavior is realized. The results obtained show that at $\approx 37\%$, the coercive field and squareness depended more strongly on the length of the NWs (or n) than on the NWs' diameter for both types of samples. Thus, based on the analysis of the experimental data, it can be assumed that such factors as size effects and magnetostatic interaction between

NWs, implemented in the system Ni/MPAA, contribute to the change in the magnetic parameters of the system as a whole. However, to determine the influence of each of them separately on this stage of the study is not possible, and investigations on this urgent topic are continuing.

Author Contributions: Conceptualization, A.V., D.T. and A.T. (Alex Trukhanov); methodology, A.V.; software, M.D.; validation, M.I.S., M.D. and A.K. (Alexander Kislyuk); formal analysis, E.K. and M.Z.; investigation, A.V., D.T. and D.S.; resources, I.K.; data curation, M.I.S.; writing—original draft preparation, A.V., D.T. and T.Z.; writing—review and editing, D.V., A.T. (Alex Trukhanov), A.V., and D.T.; visualization, A.K. (Artem Kozlovskiy) and M.D.; supervision, D.T. and A.V.; project administration, A.T. (Andrei Turutin) and I.K.; funding acquisition, A.T. (Andrei Turutin). All authors have read and agreed to the published version of the manuscript.

Funding: An.T. (Andrei Turutin) acknowledges the financial support of the Russian Science Foundation (Grant No. 19-79-30062) in part of the experimental work. A.K. (Alexander Kislyuk) and I.K. (Ilya Kubasov) acknowledge the financial support of the Ministry of Science and Higher Education of the Russian Federation as a part of the State Assignment (basic research, Project No. 0718-2020-0031 “New magnetoelectric composite materials based on oxide ferroelectrics having an ordered domain structure: production and properties”) in part of the XRD study.

Institutional Review Board Statement: Not applicable.

Informed Consent Statement: Informed consent was obtained from all subjects involved in the study.

Data Availability Statement: The data presented in this study are available on request from the corresponding authors.

Acknowledgments: D.V. (Denis Vinnik) thanks the system of the President’s grants for young doctors of science (MD-5612.2021.4) for putting facilities at the author’s disposal.

Conflicts of Interest: The authors declare no conflict of interest.

References

1. Mátéfi-Tempfli, S.; Mátéfi-Tempfli, M.; Vlad, A.; Antohe, V.; Piraux, L. Nanowires and nanostructures fabrication using template methods: A step forward to real devices combining electrochemical synthesis with lithographic techniques. *J. Mater. Sci. Mater. Electron.* **2009**, *20*, S249–S254. [\[CrossRef\]](#)
2. Poinern, J.; Gerrard, E.; Nurshahidah, A.; Fawcett, D. Progress in nano-engineered anodic aluminum oxide membrane development. *Materials* **2011**, *4*, 487–526. [\[CrossRef\]](#) [\[PubMed\]](#)
3. Vorobjova, A.; Labunov, V.; Shulitski, B. Chapter 4—Carbon nanotube-based composites synthesized using porous aluminum oxide. In *Research and Innovation in Carbon Nanotube-Based Composites*; The World Academic Publishing Co., Ltd.: Hong Kong, China, 2015; pp. 35–65.
4. Tishkevich, D.I.; Vorobjova, A.I.; Vinnik, D.A. Template assisted Ni nanowires fabrication. *Mater. Sci. Forum.* **2019**, *946*, 235–241. [\[CrossRef\]](#)
5. Keller, F.; Hunter, M.S.; Robinson, D.L. Structural features of oxide coatings on aluminum. *J. Electrochem. Soc.* **1953**, *100*, 411–418. [\[CrossRef\]](#)
6. Martin, C.R. Nanomaterials: A membrane-based synthetic approach. *Science* **1994**, *266*, 1961–1966. [\[CrossRef\]](#)
7. Vorobjova, A.; Tishkevich, D.; Shimanovich, D.; Zdorovets, M.; Kozlovskiy, A.; Zubar, T.; Vinnik, D.; Dong, M.; Trukhanov, S.; Trukhanov, A.; et al. Electrochemical behaviour of Ti/Al₂O₃/Ni nanocomposite material in artificial physiological solution: Prospects for biomedical application. *Nanomaterials* **2020**, *10*, 173. [\[CrossRef\]](#)
8. Sun, L.; Searson, P.C. Electrochemical deposition of nickel nanowire arrays in single-crystal mica films. *Appl. Phys. Lett.* **1999**, *74*, 2803. [\[CrossRef\]](#)
9. Fleischer, R.P.; Price, P.B.; Walker, R.M. *Nuclear Tracks in Solids: Principles and Applications*; University of California Press: Berkeley, CA, USA, 1975; p. 605.
10. Kaniukov, E.Y.; Shumskaya, A.E.; Kozlovskiy, A.L.; Zdorovets, M.V.; Trukhanov, A.V.; Zubar, T.I.; Tishkevich, D.I.; Vinnik, D.A.; Khairtadinova, D.R.; Evstigneeva, S.A.; et al. Structure and magnetic properties of FeCo nanotubes obtained in pores of ion track templates. *Nano-Struct. Nano-Obj.* **2021**, *26*, 1000691.
11. Thurn-Albrecht, T.; Schotter, J.; Kastle, G.A.; Emley, N.; Shibauchi, T.; Krusin-Elbaum, L.; Guarini, K.; Black, C.T.; Tuominen, M.T.; Russell, T.P. Ultra-high density arrays of magnetic nanostructures from diblock copolymer templates. *Science* **2000**, *290*, 2126–2129. [\[CrossRef\]](#)

12. Yakimchuk, D.V.; Bundyukova, V.D.; Ustarroz, J.; Terryn, H.; Baert, K.; Kozlovskiy, A.L.; Zdorovets, M.V.; Khubezhov, S.A.; Trukhanov, A.V.; Trukhanov, S.V.; et al. Morphology and microstructure evolution of gold nanostructures in the limited volume porous matrices. *Sensors* **2020**, *20*, 4397. [[CrossRef](#)]
13. Bundyukova, V.D.; Yakimchuk, D.V.; Kozlovskiy, A.; Shlimas, D.I.; Tishkevich, D.I.; Kaniukov, E.Y. Synthesis of gold nanostructures using wet chemical deposition in SiO₂/Si template. *Lith. J. Phys.* **2019**, *59*, 139–145. [[CrossRef](#)]
14. Yakimchuk, D.V.; Khubezhov, S.A.; Bundyukova, V.D.; Kozlovskiy, A.L.; Zdorovets, M.V.; Shlimas, D.I.; Tishkevich, D.I.; Kaniukov, E.Y. Copper nanostructures into pores of SiO₂/Si template: Galvanic displacement, chemical and structural characterization. *Mater. Res. Express* **2019**, *6*, 105058. [[CrossRef](#)]
15. Kozlovskiy, A.; Golota, I.; Zdorovets, M.; Tishkevich, D.; Zubar, T.; Trukhanov, A. The effect of the applied potentials difference on the phase composition of Co nanowires. *J. Magn. Magn. Mater.* **2021**, *517*, 167382. [[CrossRef](#)]
16. Méndez, M.; González, S.; Vega, V.; Teixeira, J.M.; Hernando, B.; Luna, C.; Prida, V.M. Ni-Co alloy and multisegmented Ni/Co nanowire arrays modulated in composition: Structural characterization and magnetic properties. *Crystals* **2017**, *7*, 66. [[CrossRef](#)]
17. Tishkevich, D.I.; Vorobjova, A.I.; Vinnik, D.A. Formation and corrosion behavior of nickel/alumina nanocomposites. *Solid State Phenom.* **2020**, *299*, 100–106. [[CrossRef](#)]
18. Lee, W.; Park, S.J. Porous anodic aluminum oxide: Anodization and templated synthesis of functional nanostructures. *Chem. Rev.* **2014**, *114*, 7487–7556. [[CrossRef](#)]
19. Srivastav, A.K. On the temperature dependent magnetization in dual-phase Co nanowires confinedly electrodeposited inside nanoporous alumina membrane. *J. Cryst. Growth* **2021**, *562*, 126084. [[CrossRef](#)]
20. Tishkevich, D.I.; Grabchikov, S.S.; Lastovskii, S.B.; Trukhanov, S.V.; Zubar, T.I.; Vasin, D.S.; Trukhanov, A.V.; Kozlovskiy, A.L.; Zdorovets, M.M. Effect of the Synthesis Conditions and Microstructure for Highly Effective Electron Shields Production Based on Bi Coatings. *ACS Appl. Energy Mater.* **2018**, *1*, 1695–1702. [[CrossRef](#)]
21. Xu, Q.; Meng, G.; Han, F. Porous AAO template-assisted rational synthesis of largescale 1D hybrid and hierarchically branched nanoarchitectures. *Prog. Mater. Sci.* **2018**, *95*, 243–285. [[CrossRef](#)]
22. Tishkevich, D.I.; Vorobjova, A.I.; Trukhanov, A.V. Thermal stability of nano-crystalline nickel electrodeposited into porous alumina. *Solid State Phenom.* **2020**, *299*, 281–286. [[CrossRef](#)]
23. Vorobjova, A.; Tishkevich, D.; Shimanovich, D.; Zubar, T.; Astapovich, K.; Kozlovskiy, A.; Zdorovets, M.; Zhaludkevich, A.; Lyakhov, D.; Michels, D.; et al. The influence of the synthesis conditions on the magnetic behaviour of the densely packed arrays of Ni nanowires in porous anodic alumina membranes. *RSC Adv.* **2021**, *11*, 3952. [[CrossRef](#)]
24. Susano, M.; Proenca, M.P.; Moraes, S.; Sousa, C.T.; Araújo, J.P. Tuning the magnetic properties of multisegmented Ni/Cu electrodeposited nanowires with controllable Ni lengths. *Nanotechnology* **2016**, *27*, 335301. [[CrossRef](#)]
25. Guerra, Y.; da Silva, J.F.O.; Viana, B.C.; Padron-Hernandez, E. Dipolar magnetic interactions in 3×3 arrays of rectangular Ni nanopillars. *Phys. E Low Dimens. Syst. Nanostruct.* **2021**, *126*, 114439. [[CrossRef](#)]
26. Kuznetsova, T.A.; Zubar, T.I.; Lapitskaya, V.A.; Sudzilouskaya, K.A.; Chizhik, S.A.; Didenko, A.L.; Svetlichnyi, V.M.; Vylegzhanina, M.E.; Kudryavtsev, V.V.; Sukhanova, T.E. Tribological properties investigation of the thermoplastic elastomers surface with the AFM lateral forces mode. *IOP Conf. Ser. Mater. Sci. Eng.* **2017**, *256*, 012022. [[CrossRef](#)]
27. Piraux, L. Magnetic nanowires. *Appl. Sci.* **2020**, *10*, 1832. [[CrossRef](#)]
28. Trukhanov, A.V.; Kozlovskiy, A.L.; Ryskulov, A.E.; Uglov, V.V.; Kislitsin, S.B.; Zdorovets, M.V.; Trukhanov, S.V.; Zubar, T.I.; Astapovich, K.A.; Tishkevich, D.I. Control of structural parameters and thermal conductivity of BeO ceramics using heavy ion irradiation and post-radiation annealing. *Ceram. Int.* **2019**, *45*, 15412–15416. [[CrossRef](#)]
29. Sousa, C.T.; Leitao, D.C.; Proenca, M.P.; Apolinario, A.; Correia, J.G.; Ventura, J.; Araujo, J.P. Tuning pore filling of anodic alumina templates by accurate control of the bottom barrier layer thickness. *Nanotechnology* **2011**, *22*, 315602. [[CrossRef](#)] [[PubMed](#)]
30. Proenca, M.P.; Sousa, C.T.; Ventura, J.; Vazquez, M.; Araujo, J.P. Ni growth inside ordered arrays of alumina nanopores: Enhancing the deposition rate. *Electrochim. Acta* **2012**, *72*, 215–221. [[CrossRef](#)]
31. Inguanta, R.; Piazza, S.; Sunseri, C. Influence of electrodeposition techniques on Ni nanostructures. *Electrochim. Acta* **2008**, *53*, 5766–5773. [[CrossRef](#)]
32. Tishkevich, D.; Grabchikov, S.; Zubar, T.; Vasin, D.; Trukhanov, S.; Vorobjova, A.; Yakimchuk, D.; Kozlovskiy, A.; Zdorovets, M.; Giniyatova, S.; et al. Early-stage growth mechanism and synthesis conditions-dependent morphology of nanocrystalline bi films electrodeposited from perchlorate electrolyte. *Nanomaterials* **2020**, *10*, 1245. [[CrossRef](#)] [[PubMed](#)]
33. Whitney, T.M.; Jiang, J.S.; Searson, P.C.; Chien, C.L. Fabrication and magnetic properties of arrays of metallic nanowires. *Science* **1993**, *261*, 1316–1319. [[CrossRef](#)]
34. Sharma, G.; Pishko, M.V.; Grimes, C.A. Fabrication of metallic nanowire arrays by electrodeposition into nanoporous alumina membranes: Effect of barrier layer. *J. Mater. Sci.* **2007**, *42*, 4738–4744. [[CrossRef](#)]
35. Tishkevich, D.I.; Grabchikov, S.S.; Grabchikova, E.A.; Vasin, D.S.; Lastovskiy, S.B.; Yakushevich, A.S.; Vinnik, D.A.; Zubar, T.I.; Kalagin, I.V.; Mitrofanov, S.V.; et al. Modeling of paths and energy losses of high-energy ions in single-layered and multilayered materials. *IOP Conf. Ser. Mater. Sci. Eng.* **2020**, *848*, 012089. [[CrossRef](#)]
36. Haehnel, V.; Fahler, S.; Schaaf, P.; Miglierini, M.; Mickel, C.; Schultz, L.; Schlörb, H. Towards smooth and pure iron nanowires grown by electrodeposition in self-organized alumina membranes. *Acta Mater.* **2010**, *58*, 2330–2337. [[CrossRef](#)]
37. Shin, S.; Kim, B.S.; Kim, K.M.; Kong, B.H.; Cho, H.K.; Cho, H.H. Tuning the morphology of copper nanowires by controlling the growth processes in electrodeposition. *J. Mater. Chem.* **2011**, *21*, 17967–17971. [[CrossRef](#)]

38. Napolskii, K.S.; Roslyakov, I.V.; Eliseev, A.A.; Petukhov, D.A.; Lukashin, A.V.; Chen, S.-F.; Liu, C.-P.; Tsirlina, G.A. Tuning the microstructure and functional properties of metal nanowire arrays via deposition potential. *Electrochim. Acta* **2011**, *56*, 2378–2384. [[CrossRef](#)]
39. Tian, F.; Zhu, J.; Wei, D.; Shen, Y.T. Magnetic Field Assisting DC Electrodeposition: General methods for high-performance ni nanowire array fabrication. *J. Phys. Chem. B* **2005**, *109*, 14852–14854. [[CrossRef](#)]
40. Chen, H.M.; Hsin, C.F.; Liu, R.S.; Hu, S.-F.; Huang, C.-Y. Controlling optical properties of aluminum oxide using electrochemical deposition. *J. Am. Chem. Soc.* **2007**, *154*, K11–K14. [[CrossRef](#)]
41. Almazan-Celis, J.; Díaz-Sánchez, L.E.; Olea-Mejía, O.F.; Piraux, L.; Medina, J.T. Ferromagnetic resonance study on the influence of the electrolytic bath acidity on the magnetic anisotropy of Ni nanowires. *J. Magn. Magn. Mater.* **2021**, *529*, 167860. [[CrossRef](#)]
42. Pirota, K.R.; Silva, E.L.; Zanchet, D.; Navas, D.; Vazquez, M.; Hernandez-Velez, M.; Knobel, M. Size effect and surface tension measurements in Ni and Co nanowires. *Phys. Rev. B* **2007**, *76*, 233410. [[CrossRef](#)]
43. Qin, L.; Zhaon, J.; Guo, Q.; Yan, Z.; Mu, F.; Chen, P.; Li, G. Effect of length on magnetic properties of Ni 300 nm wide nanowires. *Phys. E Low Dimens. Syst. Nanostruct.* **2013**, *50*, 17. [[CrossRef](#)]
44. Warcholinski, B.; Gilewicz, A.; Lupicka, O.; Kuprin, A.S.; Tolmachova, G.N.; Ovcharenko, V.D.; Kolodiy, I.V.; Sawczak, M.; Kochmanska, A.E.; Kochmanski, P.; et al. Structure of CrON coatings formed in vacuum arc plasma fluxes. *Surf. Coat. Technol.* **2016**, *309*, 920–930. [[CrossRef](#)]
45. Vorobjova, A.I.; Shimanovich, D.L.; Outkina, E.A.; Khodin, A.A. Highly ordered through-holes porous alumina membranes for nanowires fabrication. *Appl. Phys. A* **2018**, *1*, 124–132.
46. Vorobjova, A.I.; Shimanovich, D.L.; Yanushkevich, K.I.; Prischepa, S.L.; Outkina, E.A. Properties of Ni and Ni–Fe nanowires electrochemically deposited into a porous alumina template. *Beilstein J. Nanotechnol.* **2016**, *7*, 1709–1717. [[CrossRef](#)]
47. Vidal, E.V.; Ivanov, Y.P.; Mohammed, H.; Kosel, J. A detailed study of magnetization reversal in individual Ni nanowires. *Appl. Phys. Lett.* **2015**, *106*, 032403. [[CrossRef](#)]
48. Moreno, J.A.; Bran, C.; Vazquez, M.; Kosel, J. Cylindrical magnetic nanowires applications. *IEEE Trans. Magn.* **2021**, *57*. [[CrossRef](#)]
49. Trukhanov, S.V.; Trukhanov, A.V.; Panina, L.V.; Kostishyn, V.G.; Turchenko, V.A.; Trukhanova, E.L.; Trukhanov, A.V.; Zubar, T.I.; Ivanov, V.M.; Tishkevich, D.I.; et al. Temperature evolution of the structure parameters and exchange interactions in BaFe_{12-x}In_xO₁₉. *J. Magn. Magn. Mater.* **2018**, *466*, 393–405. [[CrossRef](#)]
50. Ohgai, T. Magnetoresistance of nanowires electrodeposited into anodized aluminum oxide nanochannels. In *Nanowires—Recent Advances*; Peng, X., Ed.; IntechOpen: London, UK, 2012.
51. Thongmee, S.; Pang, H.L.; Ding, J.; Lin, J.Y. Fabrication and magnetic properties of metallic nanowires via AAO templates. *J. Magn. Magn. Mater.* **2009**, *321*, 2712–2716. [[CrossRef](#)]
52. Escrig, J.; Lavín, R.; Palma, J.L.; Denardin, J.C.; Altbir, D.; Cortés, A.; Gómez, H. Geometry dependence of coercivity in Ni nanowire arrays. *Nanotechnology* **2008**, *19*, 075713–075719. [[CrossRef](#)]
53. Hwang, J.H.; Dravid, V.P.; Teng, M.H.; Host, J.J.; Elliott, B.R.; Johnson, D.L.; Mason, T.O. Magnetic properties of graphitically encapsulated nickel nanocrystals. *J. Mater. Res.* **1997**, *12*, 1076–1082. [[CrossRef](#)]
54. Du, Y.-W.; Xu, M.-X.; Wu, J.; Shi, Y.-B.; Lu, H.-X. Magnetic properties of ultrafine nickel particles. *J. Appl. Phys.* **1991**, *70*, 5903–5907. [[CrossRef](#)]
55. Pauthenrt, R. *High Field Magnetism*; Date, M., Ed.; North-Holland Publishing Company: Amsterdam, The Netherlands, 1983; p. 77.
56. Dormann, J.L.; Fiorani, D.; Tronc, E. Magnetic relaxation in fine-particle systems. *Adv. Chem. Phys.* **1997**, *98*, 283–294.
57. Vazquez, M.; Pirota, K.; Torrejon, J.; Navas, D.; Hernandez-Velez, M. Magnetic behaviour of densely packed hexagonal arrays of Ni nanowires: Influence of geometric characteristics. *J. Magn. Magn. Mater.* **2005**, *294*, 174–181. [[CrossRef](#)]
58. Martinez-Huerta, J.M.; Encinas, A.; Medina, J.T.; Piraux, L. Configuration dependent demagnetizing field in assemblies of interacting magnetic particles. *Phys. Condens. Matter.* **2013**, *25*, 226003. [[CrossRef](#)] [[PubMed](#)]
59. O’Handley, R.C. Modern magnetic materials. In *Principles and Applications*; John Wiley & Sons, Inc.: Hoboken, NJ, USA, 2000; p. 727.
60. Sun, L.; Hao, Y.; Chien, C.-L.; Searson, P.C. Tuning the properties of magnetic nanowires. *IBM J. Res. Dev.* **2005**, *49*, 79–102. [[CrossRef](#)]
61. Paulus, P.M.; Luis, F.; Kröll, M.; Schmid, G.; Jongh, L.J. Low-temperature study of the magnetization reversal and magnetic anisotropy of Fe, Ni, and Co nanowires. *J. Magn. Magn. Mater.* **2001**, *224*, 180–196. [[CrossRef](#)]
62. Karim, S.; Maaz, K. Magnetic behavior of arrays of nickel nanowires: Effect of microstructure and aspect ratio. *Mater. Chem. Phys.* **2011**, *130*, 1103–1108. [[CrossRef](#)]
63. Kartopu, G.; Yalçın, O.; Choy, K.-L.; Topkaya, R.; Kazan, S.; Aktaş, B. Size effects and origin of easy-axis in nickel nanowire arrays. *J. Appl. Phys.* **2011**, *109*, 033909. [[CrossRef](#)]
64. Demand, M.; Encinas-Oropesa, A.; Kenane, S.; Ebels, U.; Huynen, I.; Piraux, L. Ferromagnetic resonance studies of nickel and permalloy nanowire arrays. *J. Magn. Magn. Mater.* **2002**, *249*, 228–233. [[CrossRef](#)]
65. Encinas-Oropesa, A.; Demand, M.; Piraux, L.; Huynen, I.; Ebels, U. Dipolar interactions in arrays of nickel nanowires studied by ferromagnetic resonance. *Phys. Rev. B* **2001**, *63*, 104415. [[CrossRef](#)]
66. Lebecki, K.M. Modelling of magnetization reversal for long ferromagnetic nanotubes. *Mater. Sci. Pol.* **2008**, *26*, 983–988.
67. Stoner, E.C.; Wohlfarth, E.P. A mechanism of magnetic hysteresis in heterogeneous alloys. *Phil. Trans. R. Soc. Lond. A* **1948**, *240*, 599–642. [[CrossRef](#)]
68. Aharoni, A. Angular dependence of nucleation by curling in a prolate spheroid. *J. Appl. Phys.* **1997**, *82*, 1281–1287. [[CrossRef](#)]

69. Cheng-Zhang, L.; Lodder, J. The influence of the packing density on the magnetic behaviour of alumite media. *J. Magn. Magn. Mater.* **1990**, *88*, 236–246. [[CrossRef](#)]
70. Sellmyer, D.J.; Zheng, M.; Skomski, R. Magnetism of Fe, Co and Ni nanowires in self-assembled arrays. *J. Condens. Matter Phys.* **2001**, *13*, R433. [[CrossRef](#)]
71. Araujo, E.; Martínez-Huerta, J.M.; Piraux, L.; Encinas, A. Quantification of the interaction field in arrays of magnetic nanowires from the remanence curves. *J. Supercond. Nov. Magn.* **2018**, *31*, 3981–3987. [[CrossRef](#)]
72. Kawamura, G.; Muto, H.; Matsuda, A. Hard template synthesis of metal nanowires. *Front. Chem.* **2014**, *2*, 104. [[CrossRef](#)]
73. Pitzschel, K.; Bachmann, J.; Martens, S.; Montero-Moreno, J.M.; Kimling, J.; Meier, G.; Escrig, J.; Nielsch, K.; Görlitz, D. Magnetic reversal of cylindrical nickel nanowires with modulated diameters. *J. Appl. Phys.* **2011**, *109*, 033907. [[CrossRef](#)]
74. Zighem, F.; Maurer, T.; Ott, F.; Chaboussant, G. Dipolar interactions in arrays of ferromagnetic nanowires: A micromagnetic study. *J. Appl. Phys.* **2011**, *109*, 013910. [[CrossRef](#)]
75. Adeela, N.; Maaz, K.; Khan, U.; Karim, S.; Ahmad, M.; Iqbal, M.; Riaz, M.S.; Han, X.F.; Maqbool, M. Fabrication and temperature dependent magnetic properties of nickel nanowires embedded in alumina templates. *Ceram. Int.* **2015**, *41*, 12081–12086. [[CrossRef](#)]
76. Sukovatitsina, E.V.; Samardak, A.S.; Ognev, A.V.; Chebotkevich, L. Magnetic properties of nickel nanowire arrays patterned by template electrodeposition. *Solid State Phenom.* **2012**, *190*, 522–525.
77. Zeng, H.; Skomski, R.; Menon, L.; Liu, Y.; Bandyopadhyay, S.; Sellmyer, D.J. Structure and magnetic properties of ferromagnetic nanowires in self-assembled arrays. *Phys. Rev. B Condens. Matter Mater. Phys.* **2002**, *65*, 1–8. [[CrossRef](#)]
78. Leitao, D.C.; Ventura, J.; Sousa, C.T.; Pereira, A.M.; Sousa, J.B.; Vazquez, M.; Araujo, J.P. Insights into the role of magnetoelastic anisotropy in the magnetization reorientation of magnetic nanowires. *Phys. Rev. B* **2011**, *84*, 014410. [[CrossRef](#)]
79. Kumar, S.N.; Misra, R.K.; Satpal, S. Thermal expansion behavior of Ni–Al₂O₃ composites with particulate and interpenetrating phase structures: An analysis using finite element method. *Comput. Mater. Sci.* **2014**, *90*, 130–136.
80. Meneses, F.; Urreta, S.E.; Escrig, J.; Bercoff, P.G. Temperature dependence of the effective anisotropy in Ni nanowire arrays. *Curr. Appl. Phys.* **2018**, *18*, 1240–1247. [[CrossRef](#)]
81. Vorobjova, A.I.; Shimanovich, D.L.; Sycheva, O.A.; Ezovitova, T.I.; Tishkevich, D.I.; Trykhanov, A.V. Studying the thermodynamic properties of composite magnetic material based on anodic alumina. *Rus. Microelectron.* **2019**, *48*, 107–118. [[CrossRef](#)]